CHEMISTRY OF MATERIALS

ARTICLE

pubs.acs.org/cm

Uniform Large Diameter Carbon Nanotubes in Vertical Arrays from Premade Near-Monodisperse Nanoparticles

Noe T. Alvarez,[†,∥] Feng Li,[†,∥] Cary L. Pint,[‡,∥] John T. Mayo,[†,∥] Ezekial Z. Fisher,[†,∥] James M. Tour,[*,†,∥,§] Vicki L. Colvin,[*,†,∥] and Robert H. Hauge[*,†,∥]

[†]Department of Chemistry, [‡]Department of Physics and Astronomy, [§]Department of Mechanical Engineering and Materials Science, and [∥]The Richard E. Smalley Institute for Nanoscale Science and Technology, Rice University, MS 222, 6100 Main St., Houston, Texas 77005, United States

Supporting Information

ABSTRACT: Despite the many processes developed for carbon nanotube synthesis, few if any of these control the carbon nanotube diameter and length simultaneously. Here, we report a process whereby we synthesize vertically aligned carbon nanotube arrays (VA-CNT) using water-assisted chemical vapor deposition from solution processed premade and near-monodisperse iron oxide nanoparticles. Utilizing a dendrimer-assisted iron oxide nanoparticle monolayer deposition technique, the synthesis of high quality VA-CNTs is observed with a surprising degree of walls uniformity and diameters that correlate closely with the catalyst particle size. Specifically, we utilize 8.3 and 15.4 nm nanoparticle sizes to grow uniform, large diameter VA-CNTs. We observe control of the VA-CNT diameter and number of walls based on the nanoparticle size, with the 8.3 nm nanoparticles growing over 90% four-walled CNTs. Additionally, there is a sparse population of VA-CNTs with large diameters and few walls that tend to flatten into nanostructures resembling paired-layer graphene nanoribbons.

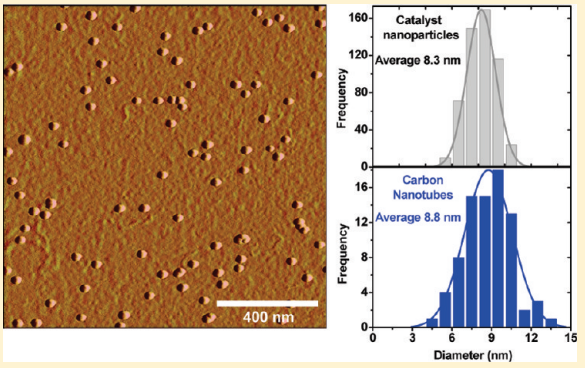

KEYWORDS: vertically aligned carbon nanotubes, catalyst, catalyst support, nanoparticles

INTRODUCTION

The synthesis of vertical arrays of carbon nanotubes (VA-CNTs) on a planar substrate is a concept that has generated significant interest.[1−3] As processing of misaligned and entangled carbon nanotubes can be challenging because of their small diameter and large aspect ratio, VA-CNT synthesis is a route where the CNTs self-assemble during growth to form a dense, aligned layer that has electrical, thermal, and mechanical properties that are appealing for a wide variety of applications.[4−7] However, many of the potential applications for VA-CNTs are limited because of an inability to control the crucial aspects of synthesis that lead to mixtures of metallic and semiconducting CNTs and CNTs having a wide range of diameters. This is largely due to the VA-CNT catalyst preparation, which is commonly achieved by the use of electron beam evaporation or sputtering to deposit a supporting oxide layer (typically 10 nm or more of Al_2O_3), and subsequently a thin catalyst layer (0.5−3 nm thick of Fe).[8,9] Upon deposition and reduction, the catalyst layer forms densely packed islands that are nucleation sites for CNT growth.[10] Since the nanoparticle size determines the nanotube diameter in most cases[11−13] this makes the definition of controlled nanoparticle sizes nearly impossible and hence, there is little or no control of nanotube diameter in this process.

An emerging process for synthesis of VA-CNTs utilizes wet-chemistry synthesis techniques to synthesize nanoparticles that are dried on oxide-layer supporting surfaces as catalysts for CNT growth.[14−16] This is advantageous in that it makes the diameter distribution of the CNTs inherently dependent on the monodispersity of the nanoparticles, and additionally provides a scalable, cost-effective route to catalyst deposition compared to e-beam evaporation. As a result, catalyst size becomes a controllable parameter that can lead to processes which result in VA-CNT structures having CNTs of uniform diameter. The use of solution processed catalyst nanoparticles for CNT growth has been utilized extensively for horizontally aligned CNT growth[17,18] and the growth of low-density CNT mats.[19] Recently, Hata's group found that "supergrowth," water-assisted growth during CVD, that results in high quality, rapid CNT growth, could be achieved with Fe−Mo solution processed nanoparticles in the same way as a catalyst layer formed using evaporation techniques.[15] However, the use of nanoparticle films for CNT growth with monodisperse nanoparticle dispersions, controlled and variable nanoparticle size, and a controllable process to form densely packed films of nanoparticles that support VA-CNT growth have yet to be described. Recently, we outlined a process for near-monolayer

Received: March 5, 2011
Revised: June 18, 2011
Published: July 07, 2011

nanoparticle film formation that can support VA-CNT growth by utilizing carboxyl terminated dendrimer films.[14]

Of all the CNTs, one of the least studied species is the large diameter CNT ($d > 4$ nm) that is typically produced in various CVD processes.[20,21] For these CNTs, the electrical properties are enhanced by temperature activation of the semiconducting species,[22] and the optical absorption features for all CNTs are shifted into the infrared,[21] which makes them challenging to study optically. Nonetheless, as the CNTs become larger, they also become less stable and are expected to collapse into tubular structures when the number of walls becomes low, similar to those documented recently by Windle's group.[23] With appreciable control of diameter and the number of walls in the CNT, this process could lead to the production of rigid multiwall carbon nanotubes (MW-CNT) structures having a controllable pore size that may be ideal for fluid transport, or thinner few-walled CNTs that could self-assemble into collapsed graphene-like materials with interesting properties. Although the latter remains unstudied, the ability to utilize carbon nanotubes to form well-defined sheets of graphene is a concept that has recently been demonstrated[24,25] and has provided synergy between research focused on the exciting properties of controllable sized graphene nanoribbons and carbon nanotubes.

Here, we demonstrate the synthesis of VA-CNTs using solution processed nanoparticles with a well-defined particle size that we called PN-NPs for "premade near-monodisperse nanoparticles" coupled with a dendrimer-assisted monolayer deposition process that produces densely packed nanoparticle films. We find that calcination is a key step to achieve high nucleation densities and optimal VA-CNT growth. Furthermore, detailed imaging studies confirm that the CNT diameter distribution is representative of the nanoparticle diameter distribution, with the controlled production of CNTs having 4 walls when utilizing 8.3 nm catalyst nanoparticles. In addition, we observe that there exists a sparse population of larger diameter, few-walled CNT species that are collapsed into structures that we denote as "tubular graphene nanoribbons." This work opens up new insight on controllable synthesis of CNTs with large diameters from homogeneous catalyst particle dispersions.

EXPERIMENTAL SECTION

All chemicals and solvents were purchased from Sigma-Aldrich and they were used without any additional treatments. The oleic acid and 1-octadecene were both 90% technical grade. The 8.3 and 15.4 nm iron oxide nanoparticles were synthesized from FeO(OH) as a precursor following our published method.[26] Typically, using a three necked flask, a mixture of FeO(OH) fine powder (0.178 g, 2.00 mmol), oleic acid (2.26 g, 8.00 mmol), and 1-octadecene (5.00 g, 0.019 mmol) was heated with stirring to 320 °C and kept at that temperature for 30 min. The nanoparticles were precipitated by adding acetone (25 mL) after cooling the mixture to room temperature. The supernatant was decanted, and the precipitated solid was then redispersed in hexanes (10 mL) with assistance of oleic acid (0.1 mL). Once synthesized, the nanoparticles were characterized by tapping mode atomic force microscopy (AFM, Veeco Metrology group, Nanoscope IIIa, Santa Barbara, CA) and transmission electron microscopy (TEM). The analytical characterizations indicated a monodisperse diameter distribution. The well-dispersed nanoparticles in hexane solution were spin coated on substrates to study their individual activity. A monolayer film of nanoparticles was assembled on an electron beam-evaporated alumina substrate using a method recently published by our lab.[14] This technique used carboxylic acid terminated polyamidoamine dendrimer (PAMAM-CO_2H) to develop a thin film of $-CO_2H$ that undergoes ligand exchange with the oleic acid ligands originally bound to the iron oxide nanoparticles.

The thin film of catalyst nanoparticles was calcined at 375 °C for different periods of time to improve their nucleation activity and therefore increase the density of CNTs in the array. The CNT growth took place in a water-assisted chemical vapor deposition reactor (CVD) apparatus with hot filament activated catalyst reduction, which has been described elsewhere.[27−29] The CNT growth protocol consists of a 30 s atomic hydrogen reduction followed by the introduction of C_2H_2, H_2O, and H_2, which were supplied during the growth period (15 min) in a manner similar to the supergrowth technique described by Hata et al.,[30] except under vacuum.[27] A total flow rate of ∼400 standard cubic centimeters per min (sccm) of H_2, 2 sccm H_2O, and 2 sccm C_2H_2 was maintained in the 1 in. tube furnace at 1.5 Torr vacuum and 750 °C.

The scanning electron microscope (SEM) images were taken with an environmental SEM (FEI Quanta 400) at 20 KV. TEM micrographs were taken with a JEOL field emission gun transmission electron microscopy. The Raman spectra were collected with an inVia micro-Raman spectrometer (Renishaw, Gluocestershire, U.K.). Diameter measurements of the CNTs were performed using digital Micrograph software.

RESULTS AND DISCUSSION

The use of iron oxide PN-NPs to form monolayers of catalyst to support VA-CNT growth is advantageous for a number of reasons. The most important reason is that particle size can be controlled prior to forming the catalyst layer; this unique control of the catalyst particle size distribution is not possible through conventional methods of metal catalyst evaporation to form self-assembled catalyst islands. This is important since control of nanoparticle size plays a key role in the diameter of the nanotube that is synthesized. To demonstrate the use of well-defined particle sizes for VA-CNT growth, we synthesized iron oxide PN-NPs with a narrow distribution of diameters, with the average size near 8.3 nm. Additionally it is worth to mention that these iron oxide PN-NPs are magnetite as they have shown their crystal structure by X-ray diffraction (XRD), see Supporting Information, Figure S1. As shown in Figure 1, these nanoparticles have been characterized extensively by AFM and TEM. After spin-coating these nanoparticles on SiO_2 at densities of ∼60 nanoparticles/μm^2, the homogeneity of the particle sizes was confirmed with AFM measurements, as depicted in Figure 1a. The height measurement of 538 iron oxide PN-NPs imaged by AFM is represented on a histogram shown in Figure 1b, which is well-fit to a Gaussian distribution having a narrow distribution and full-width half-maximum (FWHM) of 2.4 nm. This narrow particle size distribution is also observed in the TEM characterization, as is shown by a representative TEM image in Figure 1c. Additional TEM characterization is provided in the Supporting Information, Figure S2). This nearly monodisperse particle size distribution is advantageous for CNT growth, as nanoparticle size is known to play a crucial role in the diameter of the nanotube that is grown. To achieve dense VA-CNT growth, we utilized a recently developed process to construct monolayers of nanoparticles, using a carboxyl terminated dendrimer layer, where the dendrimers behave as linkers between the nanoparticles and the alumina support.[14] PAMAM-CO_2H was assembled as a monolayer film on the evaporated Al_2O_3 thin film followed by the nanoparticle assembly over the PAMAM-CO_2H film. This thin film of nanoparticles assembled with 8.3 nm iron oxide PN-NPs is shown in Figure 1d. It should be noted that the use of a chemical linker between the nanoparticles and supporting layer is an advantageous route for VA-CNT growth, as it promotes the formation of only a single layer of nanoparticles, as opposed to multilayers formed in most other coating techniques, and results

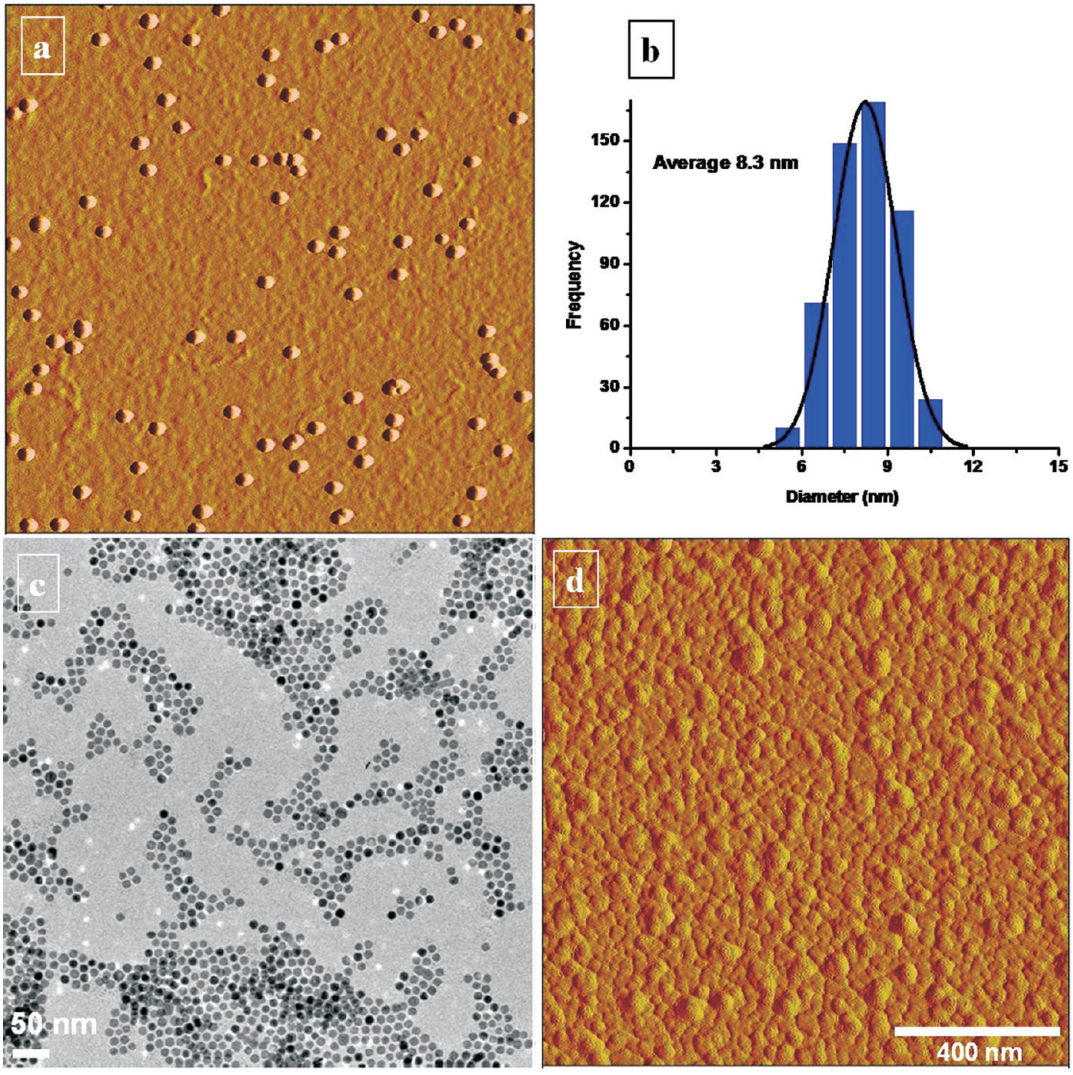

Figure 1. Characterization of 8.3 nm iron oxide PN-NP catalyst; (a) AFM images of individual PN-NPs with ~60 PN-NPs/μm^2 areal densities, (b) height measurements of 538 catalyst PN-NPs represented in a histogram with a Gaussian curve fitted on the distribution. (c) TEM images of the iron oxide PN-NP catalyst and (d) monolayer of PN-NPs assembled using PAMAM-CO_2H dendrimer.

in a stable well-packed layer of nanoparticles that are locked in place to promote nucleation and growth of a dense VA-CNT array.

Figure 2a and 2b are side-view SEM images of VA-CNT growth from dense catalyst layers similar to that shown in Figure 1d. Simply preparing the catalyst layer and exposing it to growth conditions consistently resulted in poor growth when compared to conventional VA-CNTs grown from evaporated catalyst layers. However, by exposing the catalyst layer to calcination in air (heating to 375 °C), the height of the CNT array substantially increased. Figure 2a is an image of a VA-CNT layer exposed to calcination for 2.5 h, while Figure 2b is a VA-CNT layer exposed to calcination for 20 h. Comparing the two cases, the extended calcination of the catalyst more than doubles the resulting VA-CNTs length. Initially, the goal of calcining the prepared catalyst layers was to evaporate the oleic acid capping agent from the nanoparticle surface, with the temperature based on the boiling point of oleic acid. The finding that the calcination to evaporate the capping agent produced significantly enhanced VA-CNTs growth motivated further investigation into this process.

To further investigate the role of calcination on the VA-CNT growth, we performed short growth experiments (60 s) with nanoparticle layers having similar aerial density (~60 nanoparticles/μm^2) on evaporated Al_2O_3; this is a shorter reaction time than that required to achieve VA-CNT growth. As depicted in Figure 3a and 3b, we found that the extended calcination (20 h) at 375 °C produced higher CNT nucleation density than shorter periods of calcination, a result that was consistent with the SEM and AFM data. This difference in nucleation density could be responsible for the difference in VA-CNT growth as is observed in the growth experiments depicted in Figure 2. This difference in nucleation density with calcination time could be a result of a number of factors, including evaporation of the oleic acid capping agent, catalyst support interaction on or the crystalline phase of the PN-NPs, and/or the efficiency of the reduction of the metal-oxide to a catalytically active metallic state.

To investigate the effect of reduction on the catalyst particle nucleation density, reductions were performed with N_2H_4 instead of atomic hydrogen on noncalcined catalyst. Reduction experiments were performed for 60 s at 400 and 600 °C under

dx.doi.org/10.1021/cm200664g |*Chem. Mater.* 2011, 23, 3466–3475

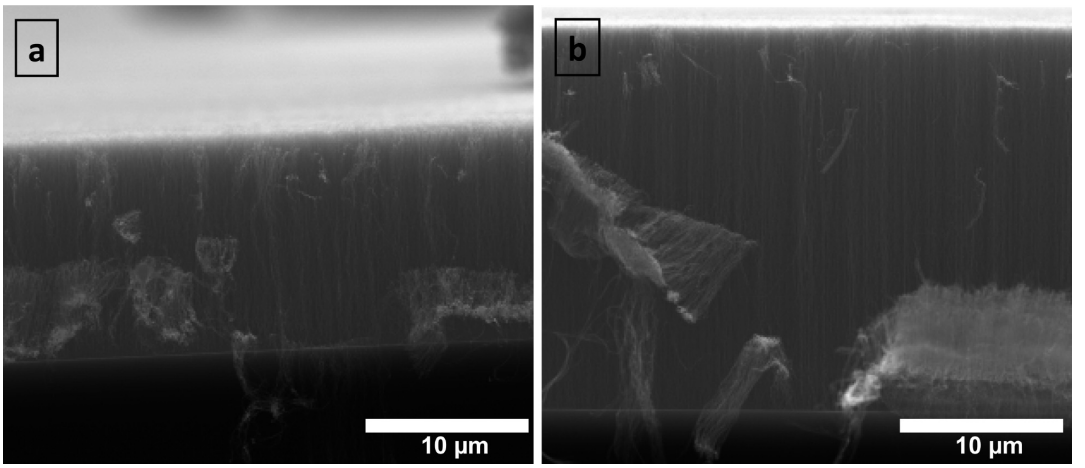

Figure 2. SEM images of VA-CNTs grown from 8.3 nm iron oxide catalyst PN-NPs with prior (a) 2.5 h of calcination and (b) 20 h of calcination before exposure to carbon flux.

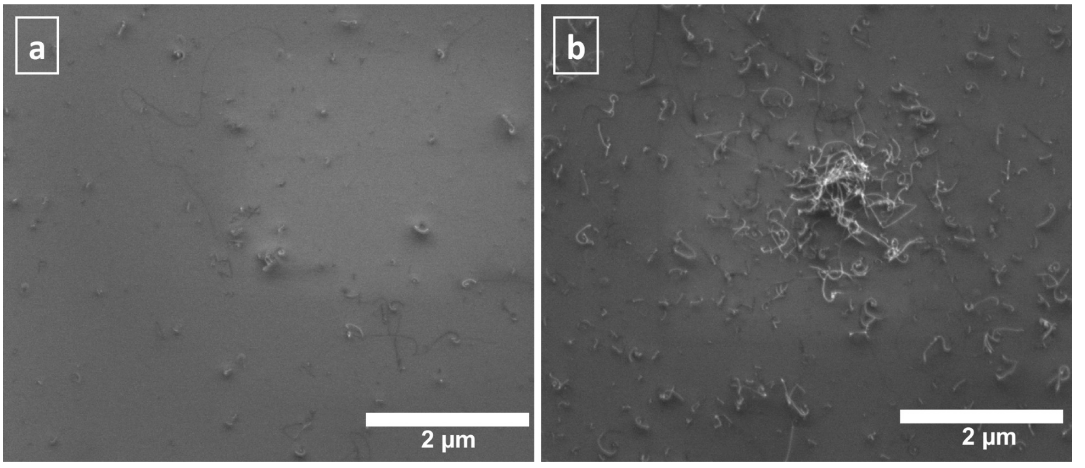

Figure 3. SEM images of similar catalyst PN-NPs areal distributions that were exposed to 60 s CNT growth environment (8.3 nm iron oxide PN-NPs) after (a) 2.5 h of calcination and (b) 20 h of calcination.

100 mTorr N_2H_4 vapor exposure in a manner similar to the process reported recently.[10] Figures 4a and 4b include SEM images that confirm that the CNT nucleation from PN-NP catalyst were significantly lower at 400 °C compared to that at 600 °C. As N_2H_4 is a highly aggressive reducing agent for metal-oxides, this provides evidence that nanoparticle reduction is important for CNT nucleation. Although N_2H_4 has been shown effective to reduce the metal-oxide to metal catalyst, in the case of PN-NP catalyst, N_2H_4 could also remove the oleic acid and promote an effective contact between the PN-NPs and Al_2O_3 substrate, thereby mimicking the effect of long calcinations. Nonetheless, we find that the treatment of the catalyst particle monolayer, either by calcination or by the use of aggressive reduction species prior to nucleation, is an integral part of achieving the high nucleation density that is coincident with the most efficient VA-CNT growth.

With the ability to achieve efficient VA-CNT growth from the PN-NP monolayers, we focused on detailed imaging and characterization of the synthesized CNTs to determine the level of control that is achieved in the use of narrow diameter distributions of nanoparticles. Figure 5a is a TEM image showing many CNTs grown in VA-CNT arrays using this technique, and Figure 5b includes a histogram that depicts the individual diameters of 93 CNTs imaged at lower magnification as in Figure 5a. Evident from Figure 5b in comparison to Figure 1b is the correlation between the CNT diameter (average = 7.4 nm, FWHM = 3.0) and the PN-NP catalyst diameter (average = 8.3 nm, FWHM = 2.5) distributions. More accurate diameter measurements were obtained with TEM at higher magnification; these TEM images indicate that the average CNT diameter is slightly higher than the average particle size, where the diameter is still strongly correlated to the particle diameter. Although the average CNT diameter is slightly lower than that of the PN-NP catalyst, slight changes to the shape or arrangement of the PN-NP catalyst and the accuracy of the measurements at this magnification could be responsible for discrepancy. Higher magnification TEM images confirm changes in catalyst shape, as shown in Figures 6a and 6b, where PN-NP catalyst found in the nanotubes are observed to be elongated. This may explain small difference in CNT diameter compared to particle diameter.

From similar high magnification images, we were able to extract the internal and external diameter of the CNTs grown from 8.3 nm nanoparticles and plot corresponding histograms of 80 CNTs, shown in Figures 6c and 6d. The internal diameter of

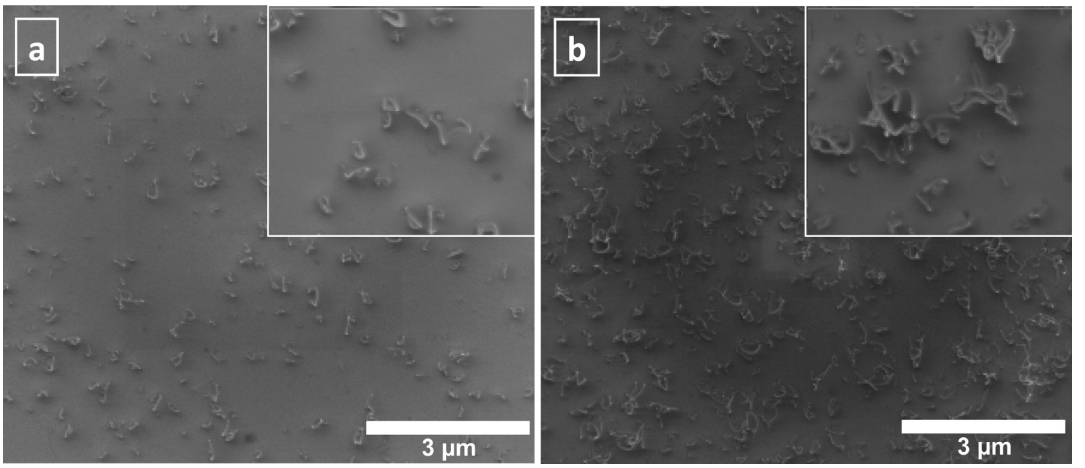

Figure 4. SEM images of similar PN-NPs areal distributions that were exposed to 60 s CNT growth environment (8.3 nm iron oxide PN-NPs) after prior (a) N_2H_4 reduction at 400 °C and (b) N_2H_4 reduction at 600 °C. The side length of the insets are 3 μm.

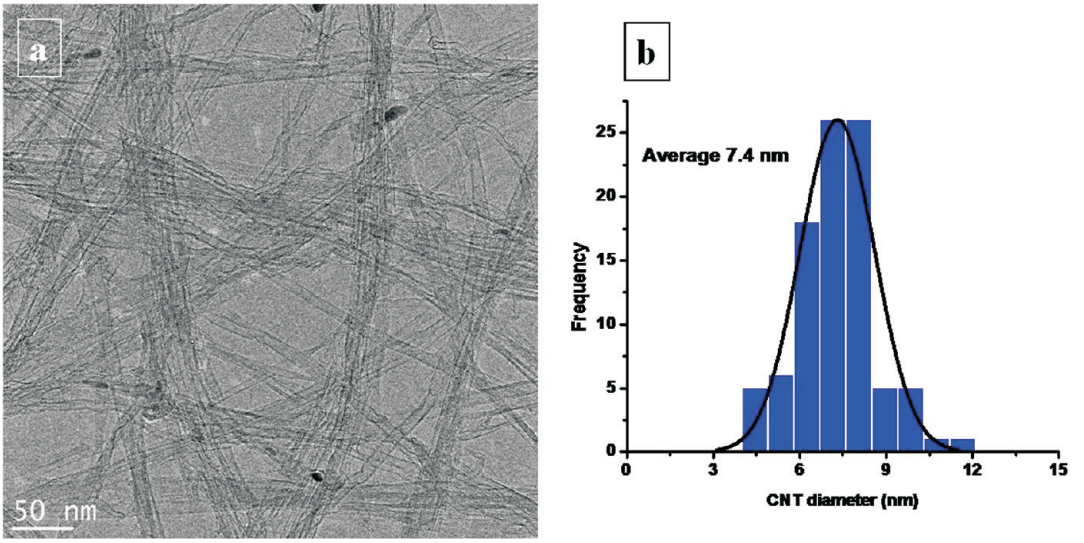

Figure 5. (a) Typical low magnification TEM images of CNTs grown from the 8.3 nm diameter PN-NPs that illustrates diameter similarity of the nanotubes to their correspondent PN-NP catalyst; (b) CNT diameter measurements represented in a histogram with an average diameter size of 7.4 nm and FWHM of 3.0 nm.

CNTs grown from PN-NP catalyst has a Gaussian distribution, with an average diameter and FWHM of 5.8 and 2.4 nm, respectively. Although the external diameter is still comparable to that of the particle distribution, the distribution is broader with an average diameter and FWHM of 8.8 and 4.2 nm, respectively. The difference between external and internal radius divided by 0.336 nm (the spacing between consecutive graphitic layers in a CNT) provides information about the number of walls. High magnification TEM images (Figure 7a) were taken from 80 tubes to construct a statistical representation of the average number of walls in the CNTs (Figure 7b). Interestingly, 90% of the CNTs had only 4 walls, with no CNTs having more than 5 or less than 3 walls. This further emphasizes the monodispersity in CNT diameter and number of walls that can be achieved with the ability to grow CNTs from monodisperse nanoparticles, and the unique correlation that exists between the CNT characteristics and the particle size.

In addition to 8.3 nm diameter PN-NP iron oxide catalyst, 15.4 nm nanoparticles were synthesized for comparison of the catalytic activity and CNT growth between the two particle sizes (see Supporting Information, Figure S3). Dendrimer-assisted iron oxide PN-NP catalyst assemblies shown by the height AFM image in Figure 8a reveals small spots with both double layers and absence of nanoparticles; however, the surface covered by a single layer coatings of iron oxide PN-NP catalyst is still predominant. In addition, the VA-CNTs grown from 15.4 nm PN-NP catalyst are significantly shorter compared to VA-CNTs grown from 8.3 nm PN-NP catalyst, with heights of only ~2 μm (Figure 8b). Despite the efforts made to activate the catalyst through extended calcinations in a manner similar to that for the 8.3 nm, 15.4 nm iron oxide PN-NP catalyst calcined for 20 h still resulted in poor growth. Similar TEM analyses performed on CNTs from 15.4 nm catalyst PN-NPs, shown in Figures 9a and 9b, reveal a wider diameter distribution compared to CNTs grown from 8.3 nm PN-NP catalyst. On the basis of measurements of 43

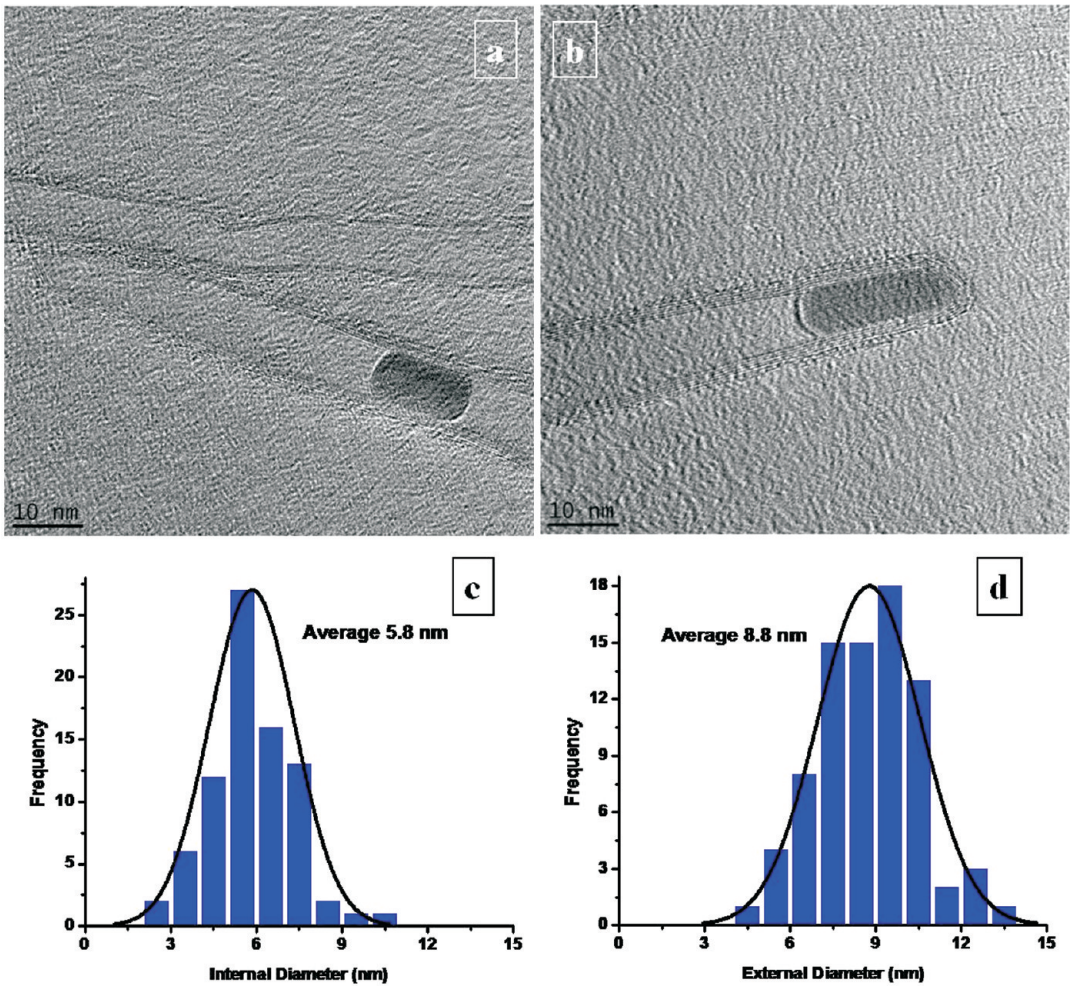

Figure 6. High resolution TEM images of CNTs grown from 8.3 nm iron oxide PN-NPs; (a) typical CNT showing the PN-NP catalyst slightly elongated and inside of the CNT, and (b) with the nanoparticle completely enclosed at the tip of the CNT. (c) Internal and (d) external diameter distribution of the CNTs represented in a histogram with diameter average of 5.8 and 8.8 nm, FWHMs of 2.4 and 4.2 nm respectively.

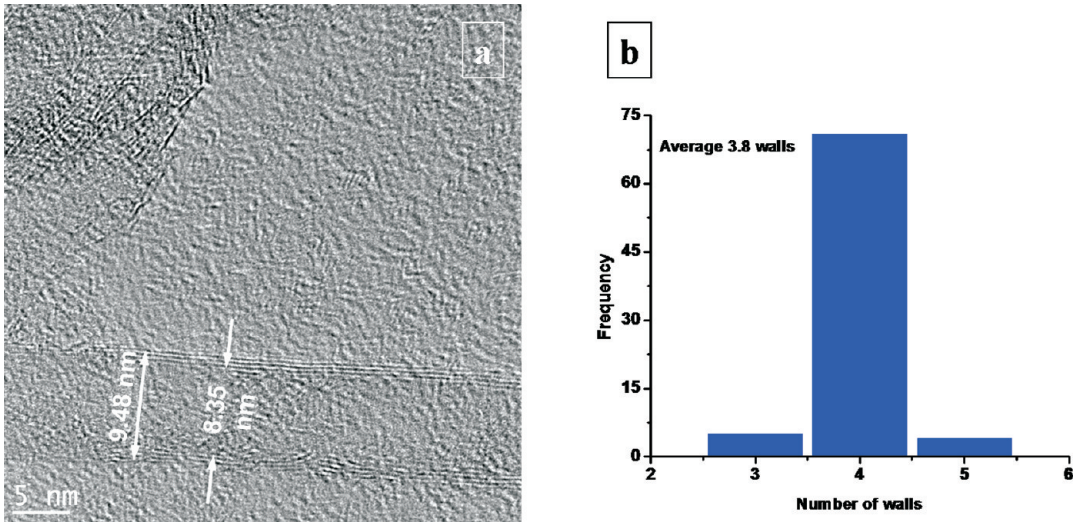

Figure 7. (a) Typical diameter measurements of the CNTs by TEM to determine their number of walls by measuring the difference between external and internal diameter. (b) Bar diagram that illustrates the number of walls of CNTs on a histogram with a Gaussian distribution fit curve, average number of walls 3.8 and 0.7 FWHM.

dx.doi.org/10.1021/cm200664g |*Chem. Mater.* 2011, 23, 3466–3475

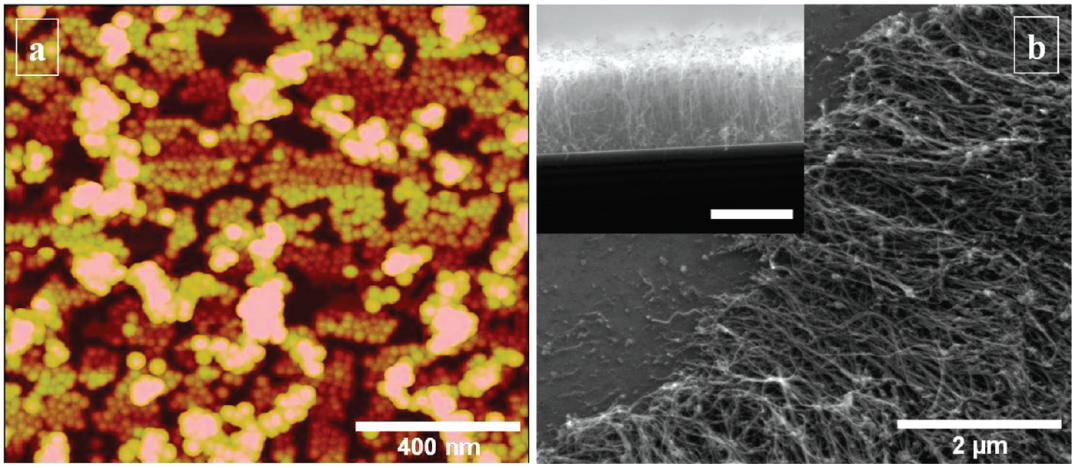

Figure 8. (a) Height AFM images of 15.4 nm iron oxide PN-NPs assembled using PAMAM-CO_2H dendrimer that reveals the nanoparticle monolayer, double layer (bright spots) and empty areas (dark spots) suggesting that despite void regions and double-layer spots, the single layer is predominant. (b) SEM of the VA-CNTs grown from monolayer of PN-NP catalyst shown in panel a. Inset illustrates the height of the VA-CNTs; inset scale bar is 2 um.

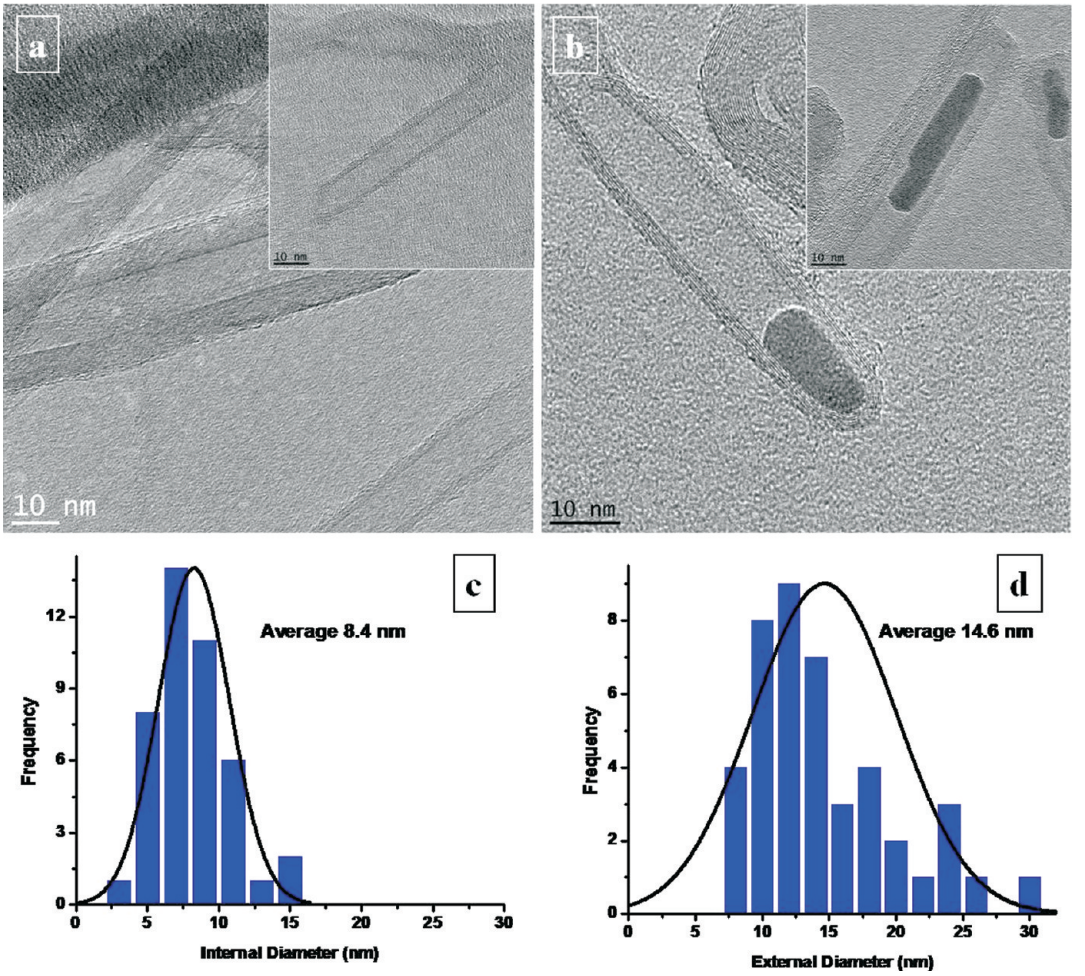

Figure 9. High resolution TEM images of CNTs grown from 15.4 nm iron oxide PN-NPs; (a) typical CNTs showing the variety of diameter and number of walls, (b) typical shapes of catalyst nanoparticles observed inside of the CNTs. (c) Internal and (d) external CNT diameter distribution represented in a histogram with FWHMs of 5.8 and 12.6 nm respectively.

CNTs grown from 15.4 nm PN-NP catalyst, it was determined that the average internal and external diameter were 8.4 and 14.6 nm, respectively, with FWHM values of 5.8 and 12.6 assuming a normal distribution. However, only the inner diameter

dx.doi.org/10.1021/cm200664g |*Chem. Mater.* 2011, 23, 3466–3475

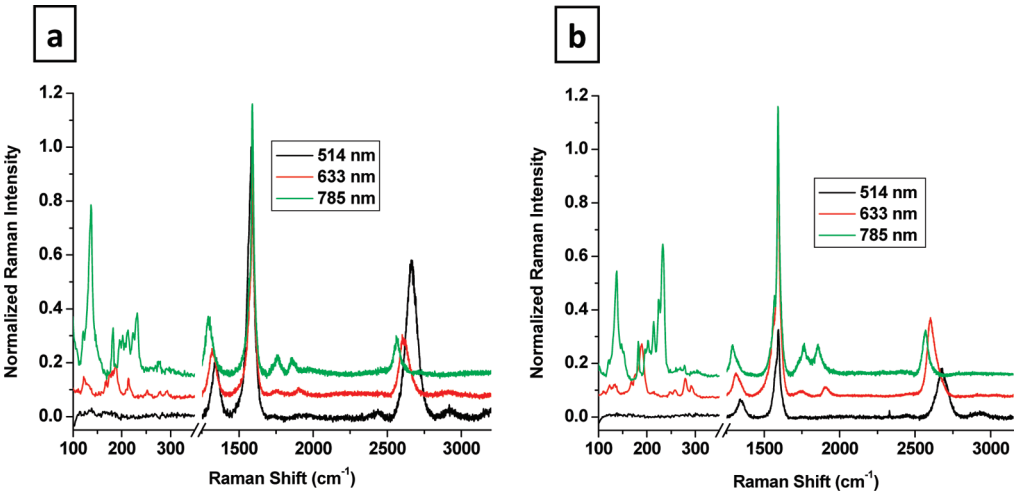

Figure 10. Raman spectra of CNTs grown from (a) 8.3 and (b) 15.4 nm iron oxide PN-NPs.

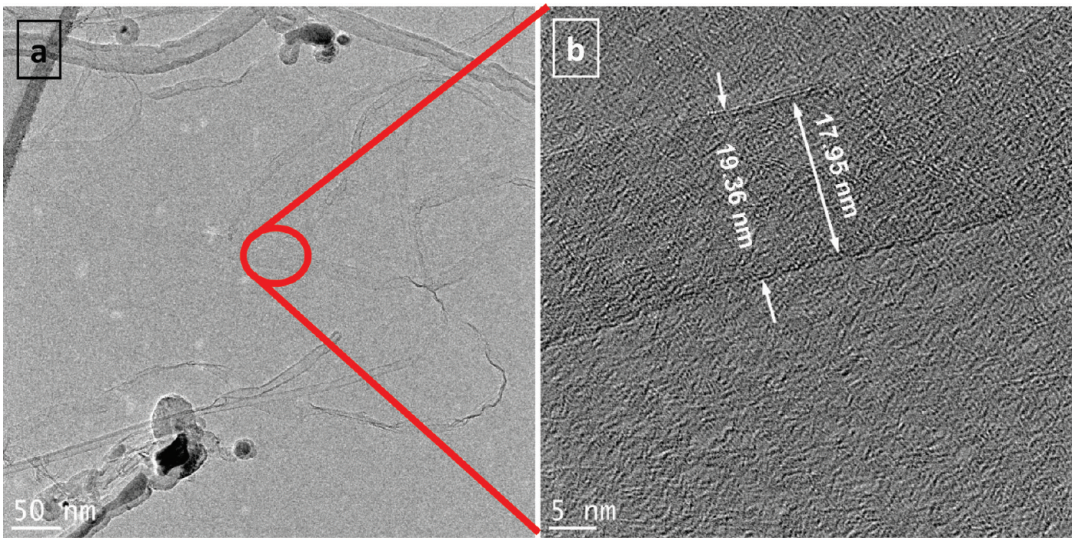

Figure 11. TEM images of CNTs grown from 15.4 nm iron oxide PN-NPs revealing collapsed CNTs forming continuous ribbon-like structures.

of the CNTs fit well to a normal distribution, while the outer diameter does not as evidenced by a diameter population larger than expected for a normal distribution. Additionally, the number of walls and the geometrical shapes of the PN-NPs, shown Figure 9b, are more diverse. Several factors in the use of the 15.4 nm PN-NPs prove to be difficult to control as compared to the 8.3 nm PN-NPs, such as the monolayer assembly of catalyst nanoparticles, and efficient nucleation activity to support VA-CNT growth. Some nonmonolayer coverage could cause particle coalescence resulting in an increase of larger diameter CNTs growth than expected for narrow particle distribution. If we neglect the larger diameter population of CNTs due to particle coalescence, it is likely that the diameter distribution would be peaked near the observed peak of ~12 nm. This indicates that CNTs grown from larger particles are likely to be somewhat smaller than the particle size. A geometrical change from spherical catalyst nanoparticles to cylindrical ones has been observed, as seen in Figures 6a, 6b, 9a and 9b. Most of the particles imaged after CNT growth have cylindrical shapes, some more absorbed into the internal diameter of the nanotube than others.

In general, we do find that the diameter distribution of the CNTs correlates well with the starting PN-NP diameter distribution with a larger deviation for the larger diameter nanoparticles. This difference may be explained by a larger elongation of the nanoparticle such as seen in the inset of Figure 9b. This is a topic that has received significant attention in recent years,[31,32] but often with conflicting results regarding whether the particle diameter is directly correlated to the CNT diameter. It should be noted that our ability to measure CNT and nanoparticle diameters with statistically accurate HR-TEM and AFM measurements tends to emphasize a striking correlation between these two features. However, additional factors, such as Ostwald ripening during the growth process, can lead to inaccuracy in postgrowth characterization of particle size compared to CNT diameter.[33,34] In addition, optical characterization techniques, such as Raman spectroscopy, used to analyze the size distributions of CNTs can often be misleading.[21] As noted elsewhere, small diameter CNTs resonate more strongly with visible and near-IR excitation, which makes these populations appear significantly enhanced. As an example of this, Raman spectra of the

dx.doi.org/10.1021/cm200664g |*Chem. Mater.* 2011, 23, 3466–3475

CNTs grown from 8.3 (Figure 10a) and 15.4 nm (Figure 10b) PN-NP catalyst have similar features to what one may expect from a sample containing small diameter CNTs, with a significant number of radial breathing modes (RBMs) present between 130 and 250 cm^{-1}. Although it is unclear whether these RBMs are indicative of small diameter CNTs, the TEM imaging did not show any such small diameter CNTs. This indicates that the small diameter CNTs are in low abundance but are the most Raman-active because of the resonance condition of the small-diameter CNTs with visible/near-IR excitation. Additionally, in the CNTs grown from 15.4 nm PN-NP catalyst, we have observed unique CNT nanostructures composed of collapsed double wall CNTs with a ribbon-like structure, as is shown in Figures 11a and 11b. It has been reported previously that a double wall CNT with a diameter above ~5 nm will collapse to form a four layer graphene ribbon-like structure with no defined edges.[35] This carbon nanostructure has a unique structure that combines features of even-layer graphene ribbons with the diameter controllability and layer commensurability that can be achieved by the CNT growth process. Although we foresee this being an exciting structure to further investigate both experimentally and theoretically, very few such structures were observed in the large diameter, few-walled VA-CNTs.

CONCLUSION

Successful VA-CNT growth from PN-NP large-diameter catalyst (8.3 and 15.4 nm) was demonstrated with a good correlation between the diameter of the catalyst nanoparticles and the CNTs. To achieve this, we found that pretreatment of the PN-NP catalyst monolayers is essential to increase nucleation densities and optimize VA-CNT growth from the catalyst monolayer assemblies. Additionally, through statistical characterization of the CNTs grown from PN-NP catalyst by HR-TEM imaging, we establish the production of near-monodisperse CNT distributions with 90% of CNTs having four walls and the CNT diameter distribution having a dispersion comparable to that of the PN-NP catalyst. Finally, we found a sparse population of few-walled, larger diameter CNTs that spontaneously collapse to form tubular graphene nanoribbons. As CNT properties are strongly correlated to diameter, there is now a clear route by which self-assembled arrays of aligned CNTs can be synthesized, thereby providing simultaneous control of CNT diameter, the number of walls in the CNTs, and CNT length. This represents a key step to produce materials for applications where CNT properties strongly influence the application performance.

ASSOCIATED CONTENT

Supporting Information. Further details are given in Figures S1−S3. This material is available free of charge via the Internet at http://pubs.acs.org.

AUTHOR INFORMATION

Corresponding Author

*E-mail: colvin@rice.edu (V.L.C.), tour@rice.edu (J.M.T.), hauge@rice.edu (R.H.H.).

ACKNOWLEDGMENT

The authors thank Erik H. Haroz, Seung Soo Lee, and Carter Kittrell for helpful discussions; Erika Bryant for assistance with CNT diameter measurements, and Aldo Frosinini for assistance with AFM imaging. This work was supported by the Air Force Research Laboratories under contract number FA8650-05-D-5807 and supported in part by the Lockheed Martin LANCER program.

REFERENCES

(1) Fan, S. S.; Chapline, M. G.; Franklin, N. R.; Tombler, T. W.; Cassell, A. M.; Dai, H. J. *Science* **1999**, *283*, 512–514.
(2) Zhang, M.; Fang, S.; Zakhidov, A. A.; Lee, S. B.; Aliev, A. E.; Williams, C. D.; Atkinson, K. R.; Baughman, R. H. *Science* **2005**, *309*, 1215–1219.
(3) Feng, C.; Liu, K.; Wu, J.-S.; Liu, L.; Cheng, J.-S.; Zhang, Y.; Sun, Y.; Li, Q.; Fan, S.; Jiang, K. *Adv. Funct. Mater.* **2010**, *20*, 885–891.
(4) Futaba, D. N.; Hata, K.; Yamada, T.; Hiraoka, T.; Hayamizu, Y.; Kakudate, Y.; Tanaike, O.; Hatori, H.; Yumura, M.; Iijima, S. *Nat. Mater.* **2006**, *5*, 987–994.
(5) Majumder, M.; Chopra, N.; Andrews, R.; Hinds, B. J. *Nature* **2005**, *438*, 44–44.
(6) Kordás, K.; Tóth, G.; Moilanen, P.; Kumpumäki, M.; Vähäkangas, J.; Uusimäki, A. *Appl. Phys. Lett.* **2007**, *90*, 123105.
(7) Ivanov, I.; Puretzky, A.; Eres, G.; Wang, H.; Pan, Z. W.; Cui, H. T.; Jin, R. Y.; Howe, J.; Geohegan, D. B. *Appl. Phys. Lett.* **2006**, *89*, 3.
(8) Christen, H. M.; Puretzky, A. A.; Cui, H.; Belay, K.; Fleming, P. H.; Geohegan, D. B.; Lowndes, D. H. *Nano Lett.* **2004**, *4*, 1939–1942.
(9) de Villoria, R. G.; Figueredo, S. L.; Hart, A. J.; Steiner, S. A.; Slocum, A. H.; Wardle, B. L. *Nanotechnology* **2009**, *20*, 8.
(10) Pint, C. L.; Kim, S. M.; Stach, E. A.; Hauge, R. H. *ACS Nano* **2009**, *3*, 1897–1905.
(11) Cheung, C. L.; Kurtz, A.; Park, H.; Lieber, C. M. *J. Phys. Chem. B* **2002**, *106*, 2429–2433.
(12) Kukovitsky, E. F.; L'Vov, S. G.; Sainov, N. A.; Shustov, V. A.; Chernozatonskii, L. A. *Chem. Phys. Lett.* **2002**, *355*, 497–503.
(13) Sinnott, S. B.; Andrews, R.; Qian, D.; Rao, A. M.; Mao, Z.; Dickey, E. C.; Derbyshire, F. *Chem. Phys. Lett.* **1999**, *315*, 25–30.
(14) Alvarez, N. T.; Orbaek, A.; Barron, A. R.; Tour, J. M.; Hauge, R. H. *ACS Appl. Mater. Interf.* **2010**, *10*, 15–18.
(15) Nishino, H.; Yasuda, S.; Namai, T.; Futaba, D. N.; Yamada, T.; Yumura, M.; Iijima, S.; Hata, K. *J. Phys. Chem. C* **2007**, *111*, 17961–17965.
(16) Gunjishima, I.; Inoue, T.; Yamamuro, S.; Sumiyama, K.; Okamoto, A. *Jpn. J. Appl. Phys.* **2007**, *46*, 3700–3703.
(17) Yuan, D.; Ding, L.; Chu, H.; Feng, Y.; McNicholas, T. P.; Liu, J. *Nano Lett.* **2008**, *8*, 2576–2579.
(18) Geblinger, N.; Ismach, A.; Joselevich, E. *Nat. Nanotechnol.* **2008**, *3*, 195–200.
(19) Ding, L.; Yuan, D.; Liu, J. *J. Am. Chem. Soc.* **2008**, *130*, 5428–5429.
(20) Futaba, D. N.; Goto, J.; Yasuda, S.; Yamada, T.; Yumura, M.; Hata, K. *J. Am. Chem. Soc.* **2009**, *131*, 15992–15993.
(21) Pint, C. L. X., Y.; Moghazy, S.; Cherukuri, T.; Alvarez, N. T.; Haroz, E. H.; Mahzooni, S.; Doorn, S. K.; Kono, J.; Pasquali, M.; Hauge, R. H. *ACS Nano* **2010**, *4*, 1131–1145.
(22) Anantram, M. P.; Leonard, F. *Rep. Prog. Phys.* **2006**, *69*, 507–561.
(23) Motta, M.; Moisala, A.; Kinloch, I. A.; Windle, A. H. *Adv. Mater.* **2007**, *19*, 3721–3726.
(24) Kosynkin, D. V.; Higginbotham, A. L.; Sinitskii, A.; Lomeda, J. R.; Dimiev, A.; Price, K.; Tour, J. M. *Nature* **2009**, *458*, 872–876.
(25) Jiao, L.; Zhang, L.; Wang, X.; Diankov, G.; Dai, H. *Nature* **2009**, *458*, 877–880.
(26) Yu, W. W.; Falkner, J. C.; Yavuz, C. T.; Colvin, V. L. *Chem. Commun.* **2004**, *20*, 2306–2307.
(27) Pint, C. L.; Pheasant, S. T.; Parra-Vasquez, A. N. G.; Horton, C.; Xu, Y.; Hauge, R. H. *J. Phys. Chem. C* **2009**, *113*, 4125–4133.
(28) Xu, Y.; Flor, E.; Kim, M. J.; Hamadani, B.; Schmidt, H.; Smalley, R. E.; Hauge, R. H. *J. Am. Chem. Soc.* **2006**, *128*, 6560–6561.

(29) Pint, C. L.; Nicholas, N.; Pheasant, S. T.; Duque, J. G.; Nicholas, A.; Parra-Vasquez, G.; Eres, G.; Pasquali, M.; Hauge, R. H. *J. of Phys. Chem. C* **2008**, *112*, 14041–14051.
(30) Hata, K.; Futaba, D. N.; Mizuno, K.; Namai, T.; Yumura, M.; Iijima, I. *Science* **2004**, *306*, 1362–1364.
(31) Moodley, P.; Loos, J.; Niemantsverdriet, J. W.; Thune, P. C. *Carbon* **2009**, *47*, 2002–2013.
(32) Schaffel, F.; Kramberger, C.; Rummeli, M. H.; Kaltofen, R.; Grimm, D.; Gruneis, A.; Mohn, E.; Gemming, T.; Pichler, T.; Buchner, B.; Rellinghaus, B.; Schultz, L. *Phys. Status Solidi A* **2007**, *204*, 1786–1790.
(33) Amama, P. B.; Pint, C. L.; McJilton, L.; Kim, S. M.; Stach, E. A.; Murray, P. T.; Hauge, R. H.; Maruyama, B. *Nano Lett.* **2009**, *9*, 44–49.
(34) Kim, S. M.; P., C. L.; Amama, P. B.; Zahkharov, D.; Hauge, R. H.; Maruyama, B.; Stach, E. A. *J. Phys. Chem. Lett.* **2010**, *1*, 918–922.
(35) Xiao, J.; Liu, B.; Huang, Y.; Zuo, J.; Hwang, K.-C.; Yu, M.-F. *Nanotechnology* **2007**, *18*, 395703.